Exploring the latest quark-meson coupling model for finite nuclei

Journal of Physics: Conference Series **1643** (2020) 012161 doi:10.1088/1742-6596/1643/1/012161

Exploring the latest quark-meson coupling model for finite nuclei

K L Martinez[1], A W Thomas[1,*], J R Stone[2,3] and P A M Guichon[4]

[1]CSSM and CoEPP, Department of Physics, University of Adelaide, SA 5005 Australia
[2]Department of Physics (Astro), University of Oxford, OX1 3RH United Kingdom
[3]Department of Physics and Astronomy, University of Tennessee, TN 37996 USA
[4]IRFU-CEA, Université Paris-Saclay, F91191 Gif sur Yvette, France

E-mail: *anthony.thomas@adelaide.edu.au

Abstract. The quark-meson coupling (QMC) model describes atomic nuclei on the basis of the quark structure of nucleons and their self-consistent change as they interact with each other in the nuclear medium. The model has been successfully applied to even-even nuclei across the entire nuclear chart and results were comparable to other existing models despite having fewer adjustable parameters. Nuclear matter properties derived from the model are also within the widely used range of values. In this paper, we explore the latest version of the model, QMCπ-II. We put some emphasis on QMC predictions for neutron skin thickness which will be the subject for experiments in the near future. QMCπ-II predicts a value of around 0.15 and 0.16 fm for ^{48}Ca and ^{208}Pb, respectively, with the slope of symmetry energy at around 40 MeV.

1. Introduction

There are number of energy density functionals (EDFs) built either in a relativistic or non-relativistic manner in the hope to better understand the structure of an atomic nuclei. The quark-meson coupling (QMC) model being one of the modern EDFs, is unusual in that it is founded on the quark structure of a hadron and its self-consistent change as it interacts with the relativistic mean-fields in the nuclear environment [1]. As a consequence, the model argues that the structure of a bound nucleon is altered in the nuclear medium contrary to the common notion that it is immutable there [2]. The QMC model offers a natural explanation of nuclear matter saturation and has been successfully used to describe dense nuclear matter such as neutron stars [3, 4].

Apart from the success of QMC in infinite nuclear matter, the model has also proved to be promising in the study of finite nuclei [5, 6, 7, 8]. It has been applied to even-even nuclei across the entire nuclear chart and QMC results for several ground-state observables were excellent despite having considerably fewer adjustable parameters compared to other existing nuclear models. QMC is unique in that at every stage of development, more physics is included in each version as the model improves. In this paper, we explore the latest QMC version, QMCπ-II when the σ meson mass, one of the model parameters, is taken at certain fixed values. We also emphasize predictions on neutron skin thickness, one of the observables of finite nuclei, which is currently of particular interest.

The paper is arranged as follows: section 2 briefly outlines the underlying theory of QMCπ-II; section 3 tackles the method of optimizing the QMC model; section 4 presents and discusses the

results obtained from QMCπ-II and in section 5 are conclusions.

2. Theory

In the QMC formalism, the NN interaction is characterized by the coupling of quark composites to the mesons in the nuclear medium. QMC utilises the MIT bag model of a nucleon where quark field equation is expressed as a function of spacetime coordinates of quarks within the bag along with the bag radius and the coupling constants of quarks to the mean scalar $\bar{\sigma}$ and vector and isovector meson fields $\bar{\omega}$ and $\bar{\rho}$ respectively. Further, the model assumes that nucleon bags do not overlap. In the following, the latest version QMCπ-II is briefly discussed.

2.1. QMCπ-II model

The derivation and the full expression of the QMCπ-II model can be found in [7]. Here we outline the major developments in the latest model. The full QMC Hamiltonian can be expressed as

$$H_{QMC} = H_\sigma + H_\omega + H_\rho + H_{so} + H_\pi \,, \tag{1}$$

where the first three terms are the contributions from the meson exchanges, H_{so} is the spin-orbit contribution arising from the model and H_π is the single-pion exchange contribution taken in the local density approximation. In QMCπ-II, higher density dependence is incorporated compared to the previous versions QMC-I [5] and QMCπ-I [6]. The effective nucleon mass is taken as

$$M_N^\star = M_N - g_\sigma \bar{\sigma} + \frac{d}{2}\left(g_\sigma \bar{\sigma}\right)^2 \tag{2}$$

as in the older versions but with the σ field solution containing ρ^2 dependence [7].

Also in this new version, the potential includes the cubic and quartic terms expressed explicitly as

$$V(\sigma) = \frac{m_\sigma^2 \sigma^2}{2} + \frac{\lambda_3}{3!}\left(g_\sigma \sigma\right)^3 + \frac{\lambda_4}{4!}\left(g_\sigma \sigma\right)^4 . \tag{3}$$

Apart from these developments, the spin-orbit part of the Hamiltonian is also improved to include spatial contributions in addition to the time components in the older versions.

2.2. Other contributions in the Hamiltonian

The total Hamiltonian of the nuclear system includes Coulomb and pairing functionals which are not part of the QMC EDF. The direct and exchange terms for Coulomb EDF is taken in its standard form

$$\mathcal{E}_{\text{Coulomb}} = e^2 \frac{1}{2} \int d^3r d^3r' \frac{\rho_p(\vec{r})\rho_p(\vec{r}')}{|\vec{r}-\vec{r}'|} - \frac{3}{4} e^2 \Big(\frac{3}{\pi}\Big)^{\frac{1}{3}} \int d^3r [\rho_p]^{4/3}, \tag{4}$$

where ρ_p is the density distribution of point-like protons.

The pairing EDF is taken in the BCS approximation throughout the nuclear volume with a delta force (DF). The functional can be expressed as [9]

$$\mathcal{E}_{\text{pair}} = \frac{1}{4} \sum_{q\in(p,n)} V_q^{\text{pair}} \int d^3r \chi_q^2, \quad \chi_{\text{q}}(\vec{r}) = \sum_{\alpha\in q} u_\alpha v_\alpha |\phi_\alpha(\vec{r})|^2, \tag{5}$$

where $q \in (p,n)$, v_α, $u_\alpha = \sqrt{1-v_\alpha^2}$ are the occupation amplitudes and α stands for quantum numbers of a single-particle state. The proton and neutron pairing strengths V_p^{pair} and V_n^{pair} are additional parameters which are fitted to experimental data apart from the QMC parameters.

3. Method

In this section, the optimization of QMC parameters and pairing strengths is discussed. Selection of data included in the fit and the algorithm used for χ^2 minimization are covered in the following subsections.

3.1. Parameter constraints

To optimize nuclear structure models, of widely used nuclear matter properties (NMPs) are the saturation point ρ_0 and the saturation energy $E_0 = E(\rho_0)$. Infinite nuclear matter is known to be bound at $\rho_0 \sim 0.16$ fm^{-3} with energy $E_0 \sim$–16 MeV. The second-order term in the expansion of $E(\rho)$ correspond to the nuclear incompressibility K_0 evaluated at ρ_0. The range for K_0 varies over a wide range from 200 – 315MeV [10, 11]. Another important description for nuclear matter is the symmetry energy S_0 and its slope L_0, as both relate to the isospin symmetry effects of the nuclear system. A summary of 28 available results from various terrestrial measurements and astrophysical observations gives S_0 from around 29 MeV to 33 MeV while L_0 has an average value of 58.9 MeV [12].

The values for ρ_0 and E_0 together with K_0, S_0 and L_0 are constraints which we impose in the fitting for QMCπ-II to determine the parameter bounds. Since there is a huge number of possible combinations of QMC parameters which satisfy the NMPs, we optimise further by fitting to observables for finite nuclei. This is discussed in the next subsection.

3.2. Finite nuclei data included in the fit

The structure of an atomic nuclei can be described through several ground-state properties. The most common quantity is the ground state binding energy, BE, with readily available data from atomic masses. Another significant observable is the charge radius, R_{ch}, taken directly from the mean-square radius of the proton distribution, assuming the protons are point-like particles. Apart from BE and R_{ch}, data is needed to constrain parameters of the pairing EDF (5), added to the QMC model. As a measure of nuclear pairing correlations, we adopt the average spectral gap $\bar{\Delta}_q$ as in [9].

There are a total of 70 doubly- and semi-magic nuclei chosen as in [13] which were included in the parameter fit for QMCπ-II. Available experimental data for BE, R_{ch} and $\bar{\Delta}_{p,n}$ for these chosen nuclei constitutes a total of 161 data points entering the fitting procedure. In the following subsection, the optimization algorithm is briefly outlined.

3.3. Optimization procedure

There are five QMC parameters and two pairing strengths which are optimized to reproduce the chosen data in subsection 3.2. This is done through a derivative-free optimization algorithm (POUNDeRS) [14] which minimizes the objective function $F(\hat{\mathbf{x}})$ or, essentially the χ^2 value, defined for QMCπ-II as

$$F(\hat{\mathbf{x}}) = \sum_{i}^{n} \sum_{j}^{o} \left(\frac{\bar{s}_{ij} - s_{ij}}{w_j} \right)^2 , \tag{6}$$

where n is the total number of nuclei, o is the total number of observables and s_{ij} and $\bar{s}_{ij}$ are the experimental and fitted values, respectively, for each nucleus i, and each observable j. w_j stands for the *effective* error for each observable, set in this fit to be $w_{BE} = 1$ MeV, $w_{R_{ch}} = 0.02$ fm and $w_{\Delta_{p,n}} = 0.12$ MeV for all nuclei. An initial parameter set $\hat{\mathbf{x}}_\mathbf{0}$ is given to POUNDeRS then it searches for the final set $\hat{\mathbf{x}}$ which gives the minimum $F(\hat{\mathbf{x}})$.

4. Results and discussion

In this section, results from the parameter optimization are presented and discussed. The fitting was carried out with fixed values of the σ meson mass from 500 – 540 MeV. This range was

chosen to satisfy the acceptable bounds for nuclear matter properties within the QMCπ-II model. Apart from the two pairing strength parameters, there are only four QMC parameters which were optimised: the coupling strengths $G_\sigma, G_\omega, G_\rho$ and λ_3.

4.1. QMCπ-II parameters and NMPs

To investigate the effects of varrying m_σ, parameter fits were done keeping m_σ at values 500 MeV, 520 MeV and 540 MeV. Table 1 shows the final parameters for each case, as well as the parameters previously obtained by taking m_σ as an adjustable parameter [8]. Table 2 presents the NMPs corresponding to the parameter sets in table 1.

Table 1. Final QMCπ-II parameter sets for fixed values of m_σ. Standard deviations are written in parentheses. The proton and neutron pairing strengths are included for completeness.

Parameters	QMCπ-II-ms500	QMCπ-II-ms520	QMCπ-II-ms540	QMCπ-II [8]	
G_σ [fm^2]	9.69	9.78	9.91	9.66	(0.02)
G_ω [fm^2]	5.29	5.53	5.74	5.23	(0.01)
G_ρ [fm^2]	4.68	4.57	4.36	4.75	(0.04)
λ_3 [fm^{-1}]	0.046	0.032	0.022	0.051	(0.001)
V_p^{pair} [MeV]	263	265	274	258	(5)
V_n^{pair} [MeV]	247	254	254	237	(5)

Table 2. Nuclear matter properties corresponding to the QMCπ-II parameters in table 1.

NMP	QMC-II-ms500	QMC-II-ms520	QMC-II-ms540	QMC-II [8]
ρ_0 [fm^{-3}]	0.15	0.15	0.15	0.15
E_0 [MeV]	-15.69	-15.72	-15.70	-15.69
a_0 [MeV]	28.8	29.0	28.7	28.8
L_0 [MeV]	41	45	45	40
K_0 [MeV]	235	249	260	230

As seen in table II of [8], m_σ has a strong negative correlation to λ_3 as well as to G_ρ. Here, it can be seen from table 1 that an increase in m_σ by 20 MeV leads to around 30% decrease in the value of λ_3. The other parameters, G_σ and G_ω as well as the pairing strengths, generally increase with m_σ. In table 2, the effect of increasing m_σ is barely seen in the values of ρ_0 and E_0 but the change is considerable for K_0. Since λ_3 effectively controls K_0 [8], the 30% decrease in λ_3 as a result of increasing m_σ, in turn leads to an increase in K_0 by around 6%. That is to say, K_0 is directly proportional m_σ. On the other hand, the symmetry energy is almost the same while its slope slightly increases with m_σ.

4.2. Fit results

We now look at the results for the finite nuclei using the QMCπ-II parameter sets presented in table 1. Figure 1 shows a comparison of absolute percent deviations from QMCπ-II with different m_σ values. It can be seen that for finite nuclei, fit results do not vary in general within the chosen m_σ. The most noticeable is in BE of $Z = 50$ isotopes where lower m_σ is favored,

while for R_{ch} of $Z = 82$ and $N = 126$, heavier m_σ is better. The QMCπ-II version also suffers higher deviations near closed shells. This will certainly be investigated and improved as the model develops.

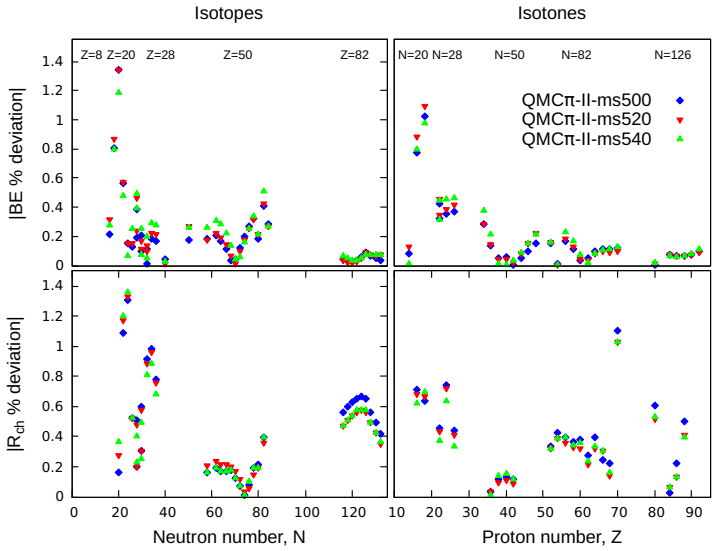

Figure 1. QMCπ-II absolute percent deviations from experiment for BE and R_{ch} of the 70 nuclei included in the fit. The plot legend is located in the top right panel.

4.3. Particle density distribution and skin thickness

A strong correlation between nuclear matter and finite nuclei has been repeatedly seen in the slope of symmetry energy L_0 and neutron skin thickness Δr_{np} [15] [16]. Δr_{np} is defined as the difference between neutron and proton geometrical radii. Various experiments and analyses have been made to determine Δr_{np} for the two doubly-magic and neutron-rich isotopes ^{48}Ca and ^{208}Pb but to date one cannot conclude with certainty as to their values. Figure 2 shows some experimental data and model predictions for ^{48}Ca and ^{208}Pb. Figure 3 shows the particle density distribution for ^{208}Pb from the QMCπ-II model and SV-min.

QMCπ-II and the covariant EDFs DD-PC1 and DD-MEδ [17] predict larger neutron skin for ^{208}Pb than ^{48}Ca contrary to the predictions from Skyrme forces SV-min [13] and UNEDF1 [18]. This behaviour can also be seen in [21] where most relativistic models predict larger skin for the lead isotope while most non-relativistic models predict otherwise. *Ab initio* coupled-cluster calculations predict ^{48}Ca neutron skin to be from 0.12 – 0.15 fm [22] while antiprotonic x-ray experiments give 0.09 ± 0.05 fm. For ^{208}Pb neutron skin, hadronic and antiprotonic x-ray experiments yielded 0.17 ± 0.02 fm and 0.15 ± 0.02 fm, respectively [20]. In figure 3, it can be seen that QMCπ-II and SV-min differ in the bulk particle distributions and that towards the surface, SV-min falls off faster compared to QMC. The upcoming CREX and PREX-II experiments at JLab are much anticipated to validate current theoretical predictions for neutron thickness and thus symmetry energy [15] and the theoretical grounds of density functional theories for the isovector sector of all nuclei in the chart [21].

5. Conclusion

The latest version for the QMC model was optimised and explored to calculate several ground-state properties of finite nuclei. The final QMCπ-II parameter sets were constrained to satisfy the acceptable range of values for NMPs while at the same time gaining very good predictions for even-even nuclei across the nuclear chart. It was seen in QMCπ-II that increasing the σ meson mass affects K_0 considerably by increasing it due to the lower λ_3 in the QMC parameters. The m_σ change, however, has a small effect on the ground-state observables of finite nuclei. We

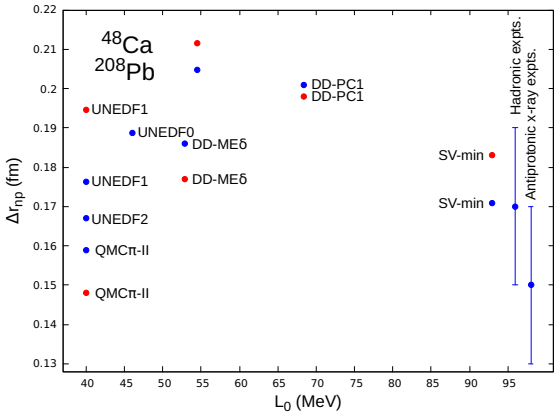

Figure 2. Δr_{np} plotted against L_0 for isotopes ^{48}Ca (red) and ^{208}Pb (blue) from QMCπ-II, DD-PC1 and DD-MEδ [17], SV-min [13], UNEDF1 [18] and UNEDF2 [19]. Also added are data from hadron scattering and antiprotonic x-ray [20] experiments.

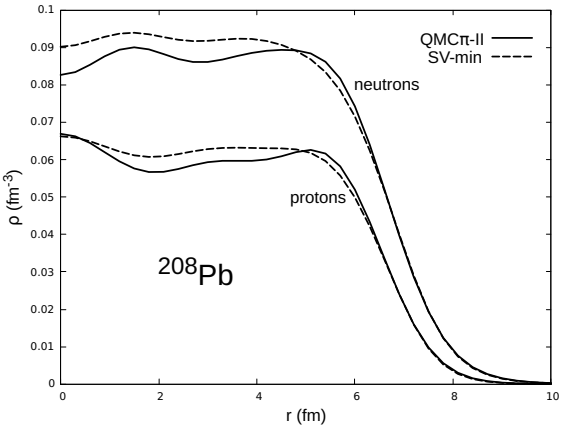

Figure 3. Proton and neutron density distributions for ^{208}Pb isotope from QMCπ-IIms500 and SV-min.

highlight the QMC predictions for neutron skin thickness as this will be subject for upcoming experiments. The best values from QMCπ-II are 0.15 fm and 0.16 fm for ^{48}Ca and ^{208}Pb, respectively, which are also within the range of existing data and other model predictions. The QMC model continues to develop and further improvements in the predictions for structure of finite nuclei are expected in the near future.

References

[1] Guichon P A M 1988 *Phys. Lett.* B **200** 235–40
[2] Thomas A W 2016 *EPJ Web Conf.* **123** 01003
[3] Stone J R, Guichon P A M, Matevosyan H H and Thomas A W 2007 *Nucl. Phys.* A **792** 341–69
[4] Thomas A W, Whittenbury D L, Carroll J D, Tsushima K and Stone J R 2013 *EPJ Web Conf.* **63** 03004
[5] Stone J R, Guichon P A M, Reinhard P G and Thomas A W 2016 *Phys. Rev. Lett.* **116**(9) 092501
[6] Stone J R, Guichon P A M and Thomas A W 2017 *EPJ Web Conf.* **163** 00057
[7] Guichon P A M, Stone J R and Thomas A W 2018 *Prog. Part. Nucl. Phys.* **100** 262–97
[8] Martinez K L, Thomas A W, Stone J R and Guichon P A M 2019 *Phys. Rev.* C **100**(2) 024333
[9] Bender M, Rutz K, Reinhard P G and Maruhn J A 2000 *Eur. Phys. J.* A **8** 59–75
[10] Stone J R, Stone N J and Moszkowski S A 2014 *Phys. Rev.* C **89**(4) 044316
[11] Dutra M, Lourenco O, Sá Martins J S, Delfino A, Stone J R and Stevenson P D 2012 *Phys. Rev.* C **85** 035201
[12] Li B A and Han X 2013 *Phys. Lett.* B **727** 276–81
[13] Klüpfel P, Reinhard P G, Bürvenich T J and Maruhn J A 2009 *Phys. Rev.* C **79**(3) 034310
[14] Kortelainen M, Lesinski T, Moré J, Nazarewicz W, Sarich J, Schunck N, Stoitsov M V and Wild S 2010 *Phys. Rev.* C **82**(2) 024313
[15] Piekarewicz J and Fattoyev F J 2019 *Physics Today* **72** 30–37
[16] Warda M, Centelles M, Vinas X and Roca-Maza X 2012 *Acta Phys. Polon.* B **43** 209
[17] Afanasjev A V and Agbemava S E 2016 *Phys. Rev.* C **93**(5) 054310
[18] Kortelainen M, McDonnell J, Nazarewicz W, Reinhard P G, Sarich J, Schunck N, Stoitsov M V and Wild S M 2012 *Phys. Rev.* C **85**(2) 024304
[19] Kortelainen M, McDonnell J, Nazarewicz W, Olsen E, Reinhard P G, Sarich J, Schunck N, Wild S M, Davesne D, Erler J and Pastore A 2014 *Phys. Rev.* C **89** 054314
[20] Trzcińska A, Jastrzębski J, Lubiński P, Kłos B, Hartmann F J, von Egidy T and Wycech S 2005 *AIP Conf. Proc.* **793** 214–21
[21] Horowitz C J, Kumar K S and Michaels R 2014 *Eur. Phys. J.* A **50** 48
[22] Hagen G *et al.* 2015 *Nature Phys.* **12** 186–90